ISTANBUL TECHNICAL UNIVERSITY ★ FACULTY OF MECHANICAL ENGINEERING

MECHANICAL ENGINEERING DEPARTMENT

AERODYNAMIC DESIGN OF A CENTRIFUGAL COMPRESSOR FOR A 500 KW TURBOCHARGER

SENIOR DESIGN PROJECT

Prepared by

030200712 Yasin YILDIZ

Advisor: Prof. Dr. Erkan AYDER

JUNE 2023

AERODYNAMIC DESIGN OF A CENTRIFUGAL COMPRESSOR FOR A 500 KW TURBOCHARGER

The aerodynamic and thermodynamic design of a 500-kW turbocharger has been successfully carried out within the scope of the graduation design project in Istanbul Technical University Mechanical Engineering Department. According to the obtained simulation results, the compressor of the turbocharger has demonstrated a highly satisfactory performance. As a result, there is a need to prepare a report solely for the compressor. This report will detail the step-by-step process of designing a centrifugal compressor to feed a turbocharger with a power of 500 kW.

THERMODYNAMIC ANALYSIS

Before designing the compressor, thermodynamic analyses were conducted, and the necessary state variables for compressor design were determined.

Isentropic compression in the compressor;

$$T_{2s} = T_1 \left(\frac{P_2}{P_1}\right)^{\frac{k-1}{k}} \quad (1)$$

Real compression in the compressor;

$$T_2 = T_1 + \frac{T_{2s} - T_1}{\eta_c} \quad (2)$$

Compressor shaft power;

$$W = \dot{m} c_p (T_2 - T_1) \quad (3)$$

Table 1: The assumption of certain fluid properties.

Variables and Constants	Compressor Fluid Properties
Cp	1.005 kJ/kg.K
k	1.4
Mass flow rate	3 kg/s

Table 2: Thermodynamic analysis

Variables and Constants	**Compressor**	
Specific shaft work	212 kJ/kg	
Shaft power	637 kW	
	Compressor Inlet	**Compressor Outlet**
Pressure	1 bar	5 bar
Temperature	20°C	231°C

DIMENSIONLESS NUMBERS

Below, some dimensionless numbers necessary for the design of the centrifugal compressor are defined.

Degree of reaction;

$$R = \frac{\Delta h_{rotor}}{\Delta h_{kademe}} \tag{4}$$

Specific diameter;

$$\delta = \frac{\psi^{1/4}}{\varphi^{1/2}} \tag{5}$$

Specific speed;

$$\sigma = \frac{\varphi^{1/2}}{\psi^{3/4}} \tag{6}$$

Work coefficient;

$$\psi = \frac{\Delta h}{\frac{U_2^2}{2}} \tag{7}$$

Flow coefficient;

$$\varphi = \frac{Q}{\frac{\pi d_2^2}{4} U_2} \tag{8}$$

Meridional flow coefficient;

$$\varphi_m = \frac{C_{m2}}{U_2} \tag{9}$$

Tangential force coefficient;

$$c_t = \frac{\psi}{\eta_{tt}\varphi_m} \tag{10}$$

DETERMINATION OF IMPELLER BASIC GEOMETRY

In compressor design, the first step is to determine the type of the compressor. For this reason, the experimental Cordier diagram is utilized, using values obtained from thermodynamic analysis and compressors dimensionless numbers. The Cordier diagram facilitates the establishment of fundamental dimensions that the compressor should possess in order to determine its type and ensure efficient operation.

Firstly, it was determined that a centrifugal compressor will be designed using the specific speed coefficient. Then, utilizing the previously defined dimensionless numbers, with the requirement for the shaft to withstand 15 MPa torsional stress at a safety factor of 1.15, and employing empirical expressions within the CFturbo (specific diameter, outlet width ratio, meridional deceleration, etc.), specific dimensions were established. However, manual adjustments were made to these dimensions.

Hub diameter, when examined for the torsional stress of the shaft to carry the torque at 20000 rpm and 640 kW power, should have a minimum diameter of 49 mm with a shear strength of 15 MPa and a safety factor of 1.15. In this design, this value was selected as 66 mm.

Impeller diameter was obtained from the Cordier diagram based on the previously mentioned specific speed and specific diameter. The diameter was selected as 506 mm.

Suction diameter was chosen as 240 mm by utilizing the meridional decrease empirical expression from the CFturbo and making manual adjustments. This 240 mm inlet diameter corresponds approximately to an 87 mm entry width.

Additionally, the definition of the mean inlet diameter is often carried out. This value is the midpoint between the inlet diameter and the hub diameter. The average inlet diameter is 153 mm.

Outlet width was calculated using the empirical expression for outlet width ratio provided in the CFturbo and was further adjusted manually. As a result, the exit width was selected as 13 mm.

The axial extension of the meridional view was calculated through empirical expressions in the CFturbo and subsequently adjusted manually, resulting in a length of 110 mm.

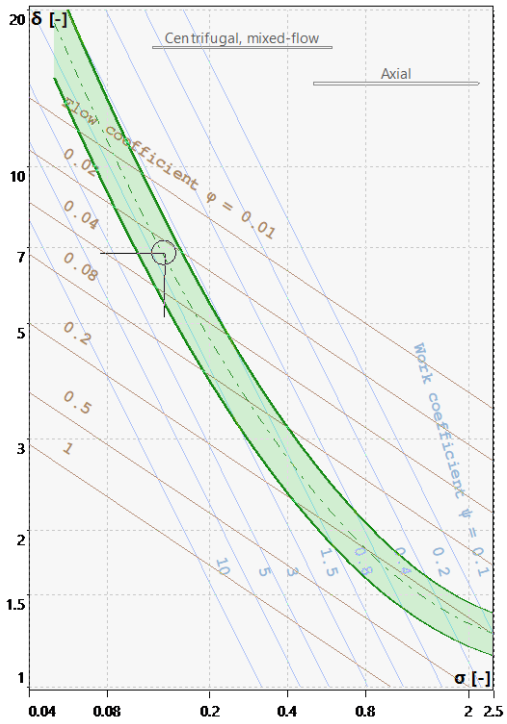

Figure 1: The designed centrifugal compressor Cordier diagram.

Table 3: Dimensions of the centrifugal compressor

Dimensions		
Hub Diameter	dH	66 mm
Suction Diameter	dS	240 mm
Mean Inlet Diameter	d1	153 mm
Inlet Width	b1	87 mm
Outlet Diameter	d2	506 mm
Outlet Width	b2	13 mm
Axial Extension	z	110 mm

The sections located on the hub and shroud sides are designed using Bezier curves. Additionally, the impeller does not encompass the entire meridional view. The blade starts from the 10% portion of the Bezier curve on the shroud side, beginning at the leading edge.

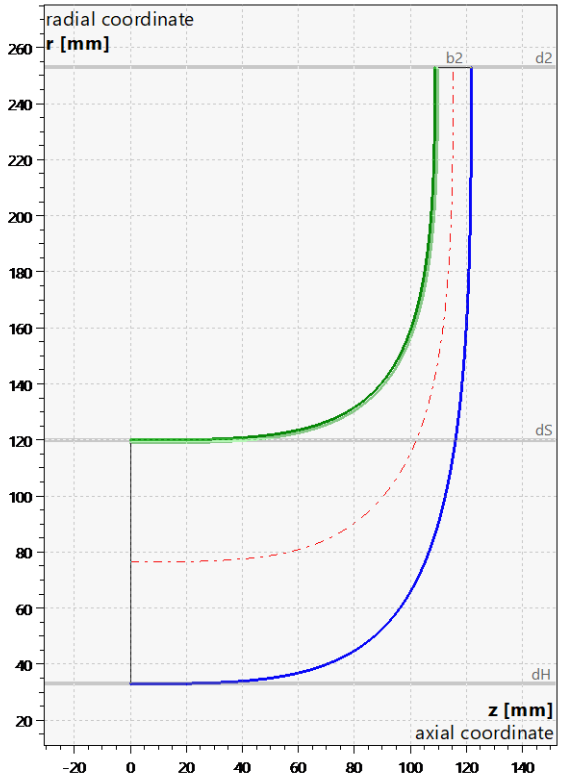

Figure 2: Meridional view of the designed centrifugal compressor

DETERMINATION OF IMPELLER VELOCITY TRIANGLES

In the previous thermodynamic analysis, the inlet and outlet thermodynamic properties of the compressor have been determined. However, these properties do not determine the dynamics the compressor must possess to achieve the calculated power. To determine this dynamics, conservation of angular momentum is first ensured, leading to the derivation of the Euler Turbomachinery equation. Subsequently, this equation is utilized to establish the dynamic characteristics of the turbomachinery.

Euler turbomachinery equation;

$$P = \omega T = \dot{m}\omega(C_{u2}r_2 - C_{u1}r_1) = \dot{m}(C_{u2}U_2 - C_{u1}U_1) \quad (11)$$

In this design, an assumption of there is no pre-swirl flow is present, thus the fluid's absolute velocity enters the compressor perpendicularly.

Inlet velocity triangle calculations can be performed using mass conservation and the definition of linear velocity.

Inlet impeller velocity;

$$U_1 = \omega\left(\frac{d_1}{2}\right) = \left(\frac{2\pi n}{60}\right)\left(\frac{d_1}{2}\right) \tag{12}$$

The perpendicular component of the fluid's inlet absolute velocity to the impeller;

$$C_{m1} = \frac{Q_1}{A_1} = \frac{\frac{\dot{m}}{\rho_1}}{\pi d_1 b_1} \tag{13}$$

The parallel component of the fluid's inlet absolute velocity to the impeller;

$$C_{u1} = 0 \tag{14}$$

Inlet absolute velocity of the fluid;

$$C_1 = \sqrt{C_{m1}^2 + C_{u1}^2} \tag{15}$$

Inlet relative velocity of the fluid;

$$W_1 = \sqrt{U_1^2 + C_1^2} \tag{16}$$

Inlet absolute velocity angle;

$$\alpha_1 = 90° \tag{17}$$

Inlet relative velocity angle;

$$\beta_1 = tan^{-1}\left(\frac{C_1}{W_1}\right) \tag{18}$$

Outlet velocity triangle calculations can be performed using mass conservation, definition of linear velocity, and the Euler turbomachinery equation.

Outlet impeller velocity;

$$U_2 = \omega\left(\frac{d_1}{2}\right) = \left(\frac{2\pi n}{60}\right)\left(\frac{d_2}{2}\right) \tag{19}$$

The perpendicular component of the fluid's outlet absolute velocity to the impeller;

$$C_{m2} = \frac{Q_2}{A_2} = \frac{\frac{\dot{m}}{\rho_2}}{\pi d_2 b_2} \tag{20}$$

The parallel component of the fluid's outlet absolute velocity to the impeller, by using Euler turbomachinery equation;

$$C_{u2} = \frac{P}{\dot{m} U_2} \tag{21}$$

Outlet absolute velocity of the fluid;

$$C_2 = \sqrt{C_{m2}^2 + C_{u2}^2} \tag{22}$$

Outlet relative velocity of the fluid;

$$W_2 = \sqrt{(U_2 - C_{u2})^2 + C_{m2}^2} \tag{23}$$

Inlet absolute velocity angle;

$$\alpha_2 = tan^{-1}\left(\frac{C_{m2}}{C_{u2}}\right) \tag{23}$$

Inlet relative velocity angle;

$$\beta_2 = tan^{-1}\left(\frac{C_{m2}}{U_2 - C_{u2}}\right) \tag{23}$$

Velocity triangles are determined on Excel using the provided equations. When compared with CFturbo, it is observed that the values are very close to each other.

Table 4: Centrifugal compressor average diameter velocity triangle values.

Velocities and Angles	
U1	160 m/s
Cu1	0 m/s
Cm1	61 m/s
C1	61 m/s
W1	172 m/s
α1	90°
β1	21°
U2	530 m/s
Cu2	401 m/s
Cm2	65 m/s
C2	406 m/s
W2	145 m/s
α2	9°
β2	27°

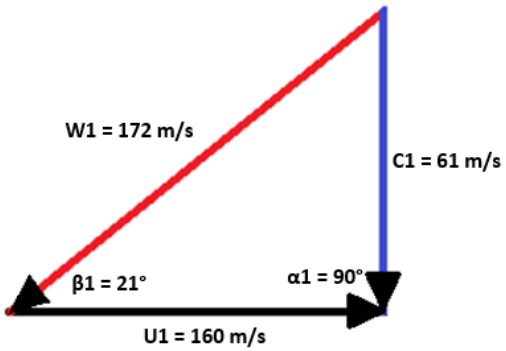

Figure 3: Mean diameter inlet velocity triangle determined by excel.

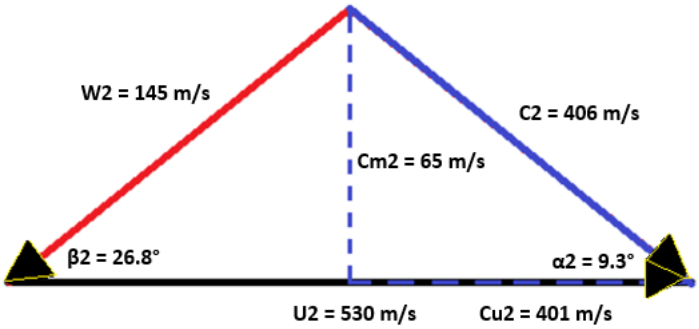

Figure 4: Mean diameter outlet velocity triangle determined by excel.

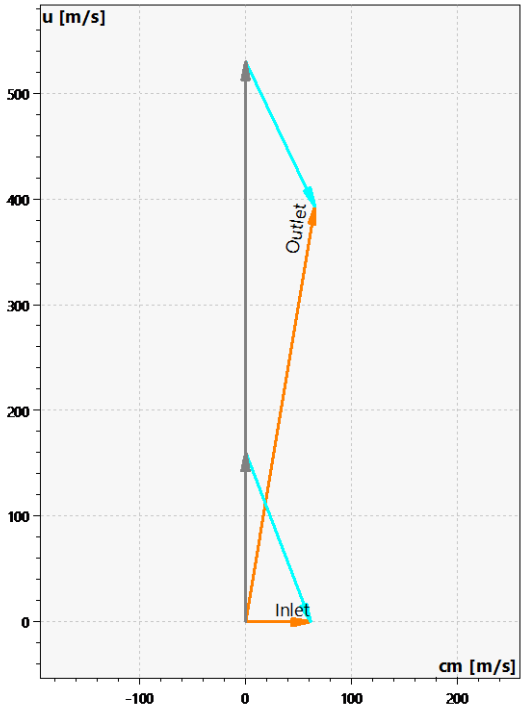

Figure 5: Mean diameter velocity triangles in CFturbo.

In this design, velocity triangle values have been calculated only at the average diameter. It is possible to obtain velocity triangles in different spans by subdividing the blade into specific small turbomachines. However, CFturbo already performs this task. The blade has been divided into 4 small turbomachines in CFturbo, resulting in obtaining velocity triangles in 5 different spans.

DETERMINATION OF IMPELLER DETAILED GEOMETRY

After obtaining the velocity triangles, the blade geometry creation phase is reached. At this stage, certain adjustments may need to be made before creating the blade geometry.

The first of these adjustments involves the angles in the velocity triangles, which directly impact performance. In this project, specific corrections will be applied to these angles. The reason for making these corrections is that the actual relative outlet angle may slightly differ from the calculated relative outlet angle. To correct this relative outlet angle in this project, the Aungier/Wiesner method embedded in the CFturbo will be utilized. After applying this method, the new relative outlet angle is calculated to be approximately 38°. In the Aungier/Wiesner approach for the slip angle in the compressor, the smaller the slip coefficient, the higher the deviation of the flow from the direction given by the blade. Aungier/Wiesner equation;

$$\gamma = 1 - \frac{C_{u2\infty} - C_{u2}}{U_2} \tag{24}$$

The second aspect in determining the geometry is how the shape of the blade will be created. This can vary widely. Due to various considerations of manufacturability, the ruled surface method is employed. This method helps form the blade surfaces on the shroud and hub. In other words, no interventions can be made to the internal spans.

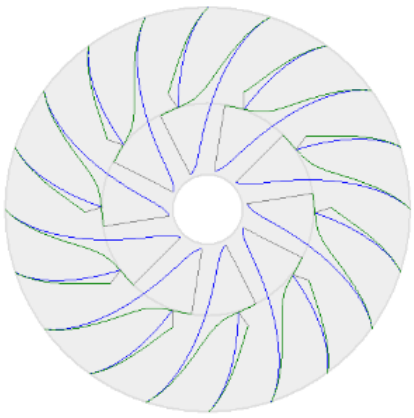

Figure 6: Ruled surface impeller.

The third aspect in determining the geometry is the blade thicknesses and blade profile. In centrifugal compressors, the blade profile doesn't have a significant impact. Compression is mainly achieved through centrifugal effects. Therefore, a flat profile is used. Profile thicknesses are set at 2.5 mm using statements available in the CFturbo to prevent blockage. Additionally, the leading and trailing edges are designed in an elliptical shape to facilitate the formation of a smoother mesh. Blockage equation is defined as;

$$B = 1 - \frac{efective\ flow\ field}{geometric\ flow\ field} \tag{24}$$

Finally, some critical parameters directly impacting the performance of the compressor have been determined as a total of 24 blade count, a wrap angle of 45°, and a rake angle of 0°. Through trial-and-error simulations, these values have been reached as optimal. The reason for this is to prevent flow separations.

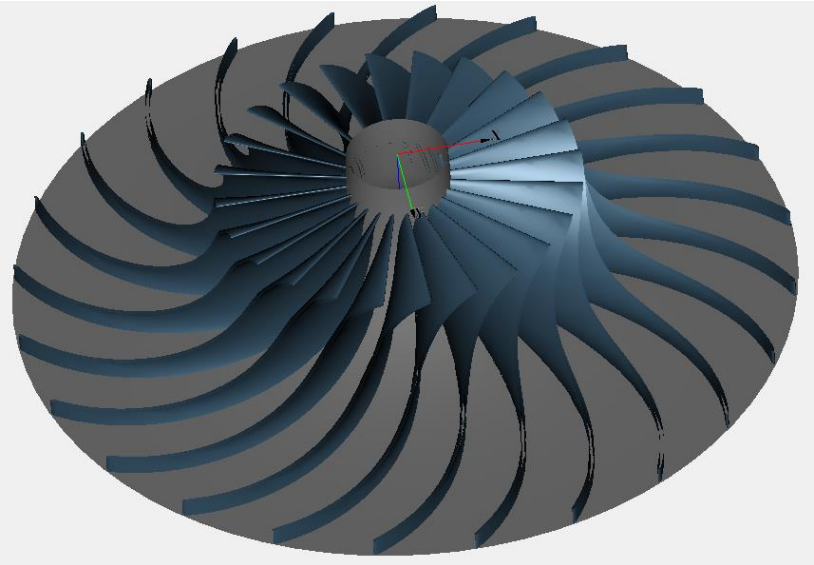

Figure 7: Impeller geometry.

DETERMINATION OF VANELESS DIFFUSER AND VOLUTE GEOMETRY

No calculation or empirical process has been carried out for the stators. A stator of 174 mm length has been directly created for the inlet. For the outlet, a diffuser with a length of 40 mm and a 2 mm widening has been generated without vanes.

For the volute, a velocity-based design has been performed using CFturbo for asymmetric round volutes. The Pfleiderer model has been used for this purpose. The diffuser has been chosen to be 400 mm in length and 140 mm in outlet diameter. Additionally, a radius of 5 mm has been added to the cutwater of the volute.

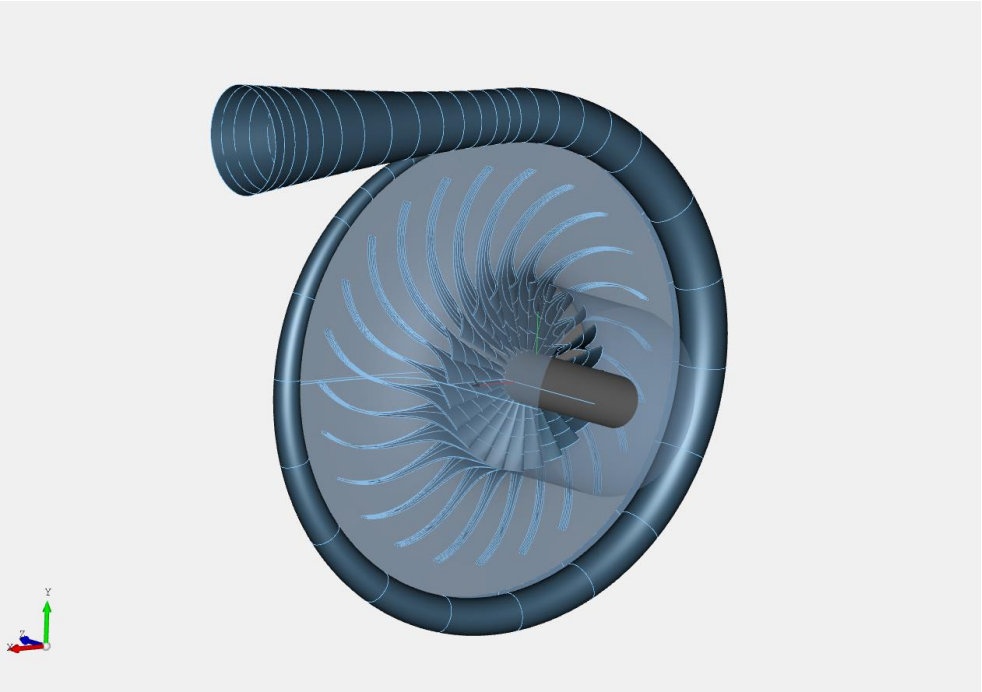

Figure 8: The obtained centrifugal compressor.

MESHING PROCESS

A mesh will be generated for a single blade using Turbogrid. Firstly, the inlet and outlet regions have been defined. Then, the topology and the number of layers in the topology have been determined. Turbogrid encompasses various topologies for turbomachinery. The 'Single Round Symmetric' topology has been selected from Turbogrid's options. Subsequently, the mesh has been created by specifying the ratios that will determine the quantity.

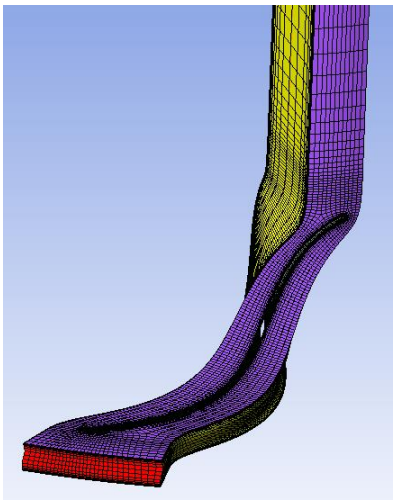

Figure 9: Generated mesh for a single blade.

Total of 71280 elements and 82720 nodes generated for a single blade geometry.

For the volute, a mesh has been generated using ANSYS Mesh with the hex-dominant method, utilizing linear elements with a length of 200 mm. In total, 42,166 elements and 32,859 nodes have been generated.

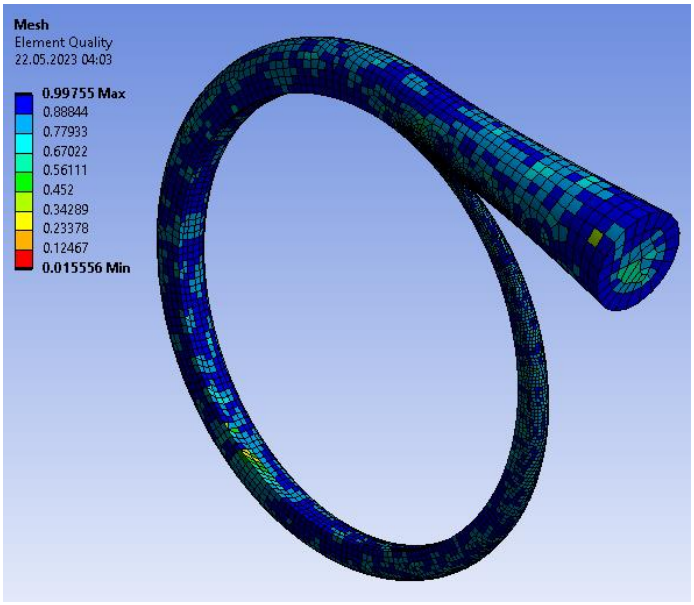

Figure 10: Generated mesh for a volute.

MODELING AND CFD PROCESS

The modeling will be conducted using ANSYS CFX Pre. The analysis type will be steady-state. Previously meshed regions have been added to the system as components. These components are divided into fixed and rotating regions. The inlet stator, outlet stator, and volute have been selected as fixed regions in the system. The rotor section has been designated as a rotating region with a speed of 20,000 RPM.

In the next stage, physical definitions have been made, encompassing fluid properties, heat transfer and turbulence models, boundary conditions, and interface models. Air has been chosen as the fluid with ideal gas properties. The total energy heat transfer model and the shear stress transport turbulence model have been employed. Boundary conditions have been defined: inlet conditions include temperature and pressure, while the outlet condition is set as mass flow rate. Inlet conditions are specified as 20 °C and 1 bar total pressure, and the mass flow rate passing through the entire machine is set to 3 kg/s at the outlet. Finally, a frozen rotor interface model has been utilized for the interface between components.

Interfaces represent the planes where the specified components interact with each other, excluding the inlet and outlet. A total of 6 interfaces have been defined. Firstly, a periodic interface has been defined for the inlet stator. Secondly, a frozen rotor interface has been defined between the inlet stator and the rotor. Thirdly, a periodic interface has been defined for the rotor. Afterwards, a frozen rotor interface has been specified between the rotor and the outlet stator. Subsequently, a periodic interface has been defined for the outlet stator. Lastly, a frozen rotor interface has been defined between the volute and the outlet stator. Additionally, the lack of symmetry in the volute, and the periodicity of the outlet stator necessitated the definition of a specific angular pitch between these two interfaces.

Apart from the inlet and outlet boundary conditions, some surfaces have been designated with boundary conditions. Non-slip wall conditions have been applied to the shroud, hub, and blades of all stators and the rotor. The volute's spiral, cutwater, and diffuser surfaces also have been set with non-slip wall conditions.

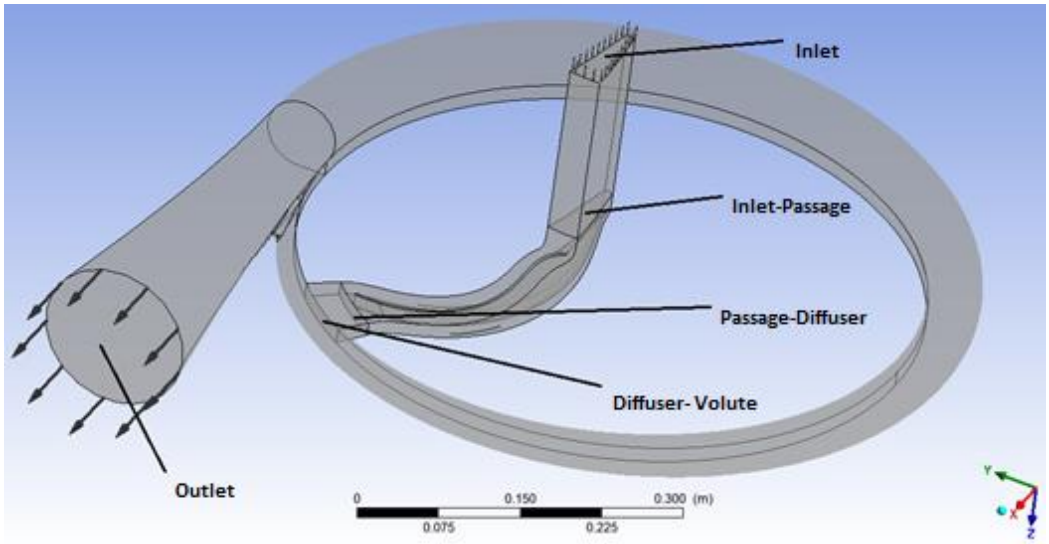

Figure 11: Generated interfaces.

This model has been utilized at 28 different off-design points besides the design point. A total of 29 different analyses have been run for all these points. Analysis results for the design point will be presented in the results section. For the points other than the design point, only the compressor performance map will be provided. For the design point, the model has been converged up to level 10^{-6}. Mass and momentum convergence curves are given in the figures. For the other points, the model has been converged at levels of 10^{-4}. Therefore, the 10^{-4} level has been identified as the instability threshold.

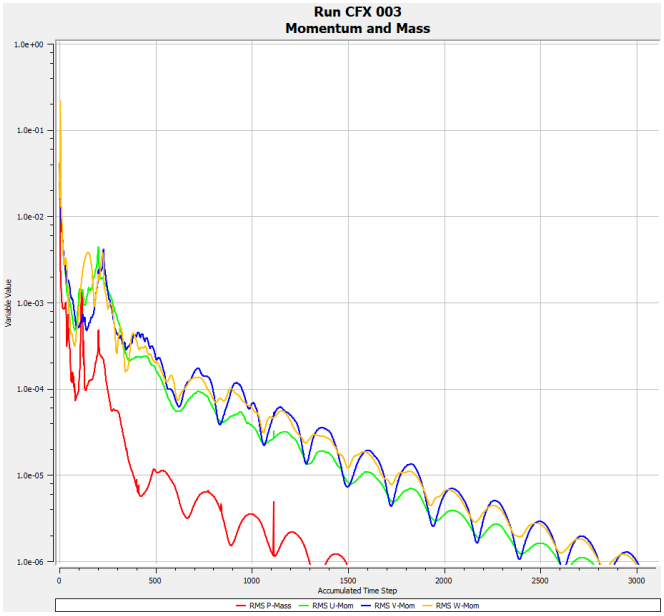

Figure 12: Convergence curves

RESULTS

As previously mentioned, CFD analyses have been conducted for the designed compressor at the design point and 28 different off-design points. All these analyses have achieved convergence below 10^{-4}. Within the scope of this project, all results except for the performance map will be provided specifically for the design point.

Table 5: CFD simulation data for some points.

Speed	Mass Flow Rate	Efficiency	Total Pressure Ratio	Total Temperature Ratio	Torque	Power	Convergence
15000 rpm	1.5 kg/s	0.797	2.75	1.42	120 J	188.4 kW	(10^-4)-(10^-6)
15000 rpm	2 kg/s	0.818	2.68	1.4	150 J	235 kW	(10^-6)
17500 rpm	2 kg/s	0.788	3.66	1.57	186 J	341 kW	(10^-4)-(10^-6)
17500 rpm	3 kg/s	0.779	3.34	1.53	253 J	465 kW	(10^-6)
20000 rpm	3 kg/s	0.795	4.95	1.73	307 J	643 kW	(10^-6)
20000 rpm	3.5 kg/s	0.815	4.94	1.71	348 J	728 kW	(10^-6)
22500 rpm	5 kg/s	0.753	6.1	1.9	564 J	1323 kW	(10^-4)-(10^-6)

The table provides some data regarding simulation results for 7 different points. Overall, the outputs of 29 different simulations can be get from the performance map.

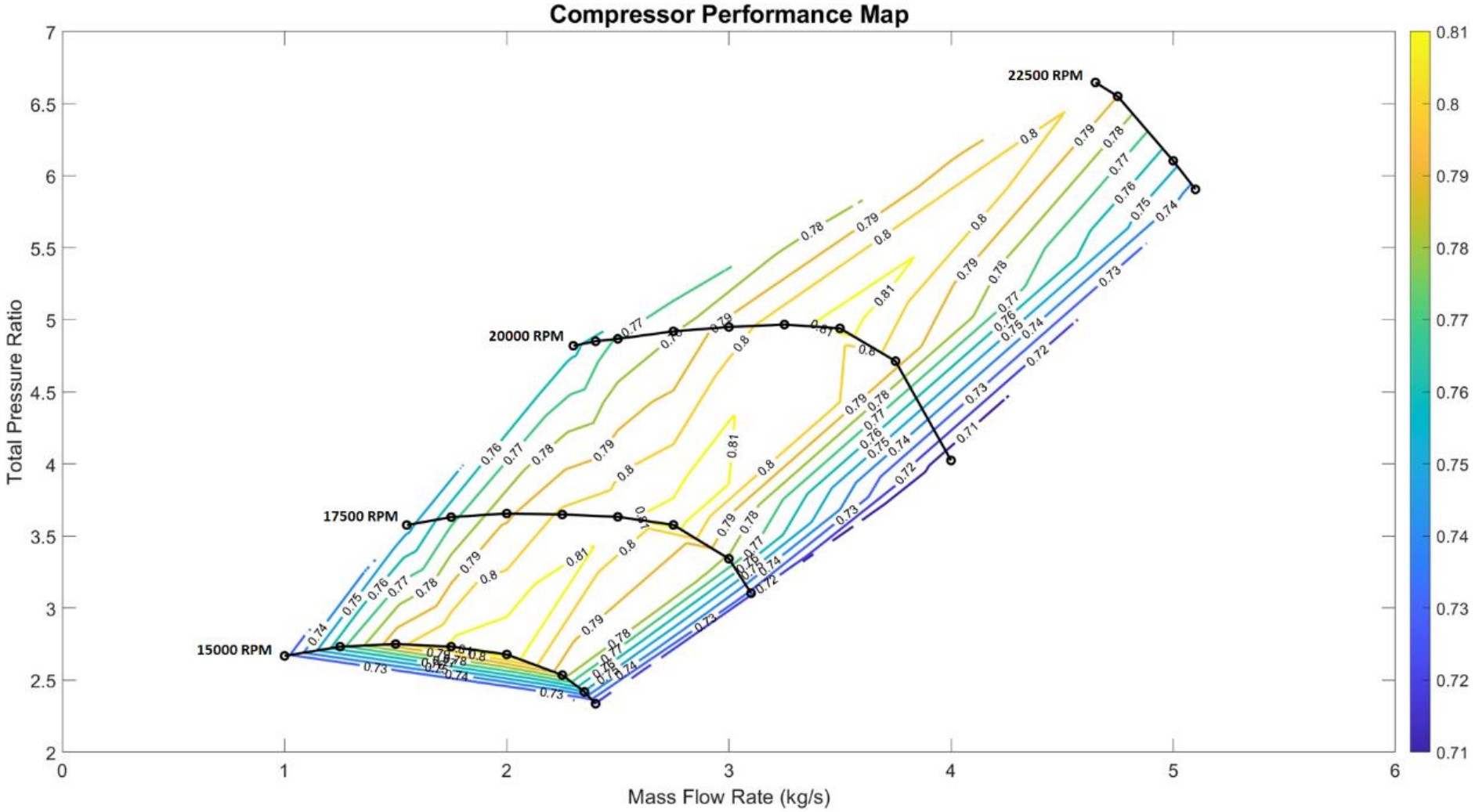

Figure 13: Compressor performance map.

In the compressor performance map, the efficiency contours are represented. Efficiency isolines do not merge at certain internal points as expected. The reason for this is the insufficient number of CFD simulations carried out at various operating points. If additional CFD simulations were conducted at intermediate speeds, better efficiency contours could have been obtained. Additionally, it is observed that the upper portion of the map is limited by the surge line, and the lower portion is bounded by the choke line due to the convergence criteria.

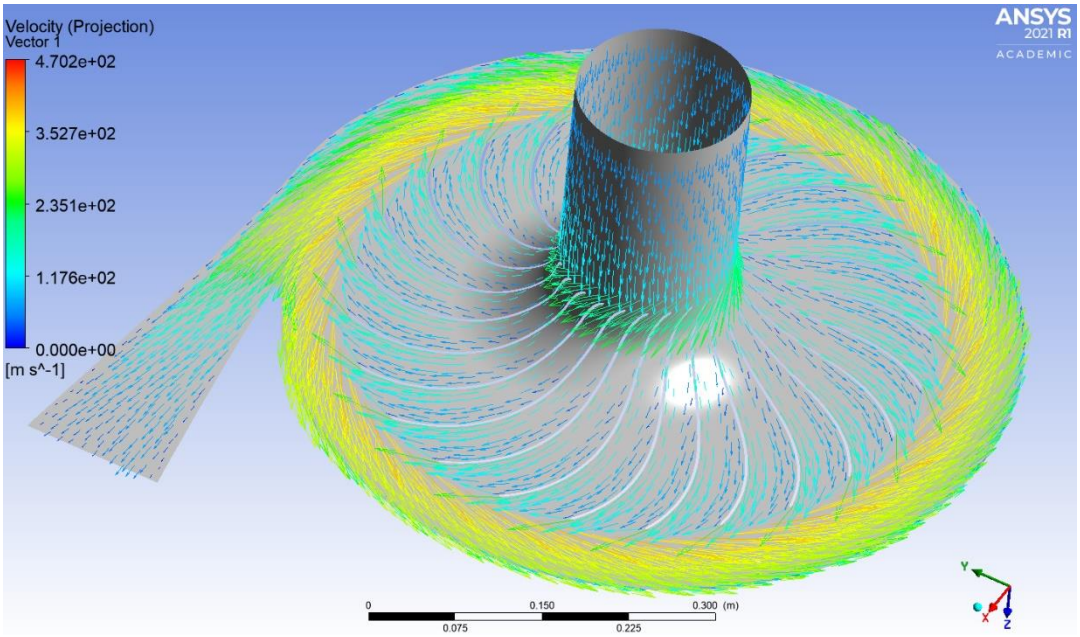

Figure 14: Tangential relative velocity vectors in the midspan of the compressor.

As seen from figure, tangential relative velocity vectors in the midspan of the compressor exhibit a very smooth distribution. Flow separations were encountered in analyses conducted with different geometries. However, as a result of the optimization performed, no flow separation is observed in the final design.

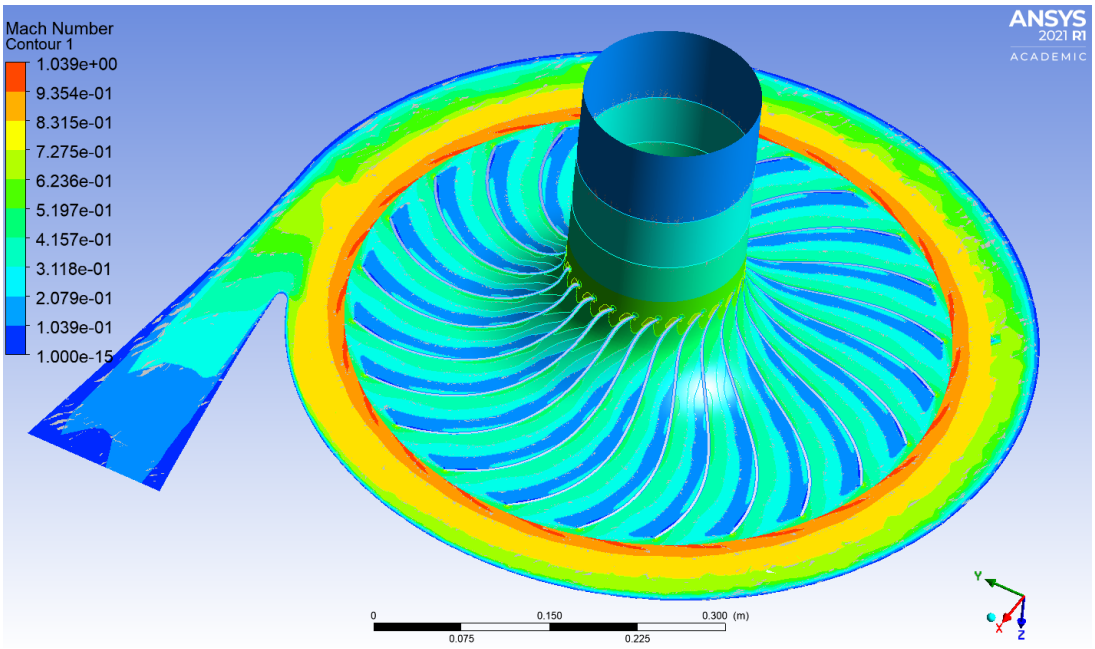

Figure 15: Local Mach numbers in the midspan of the compressor.

As seen from figure, in the midspan of the compressor, local Mach numbers reach supersonic levels at certain points. In the scope of the project, generally subsonic regions were desired, however, for a compressor of this power, locally exceeding the speed of sound is unavoidable.

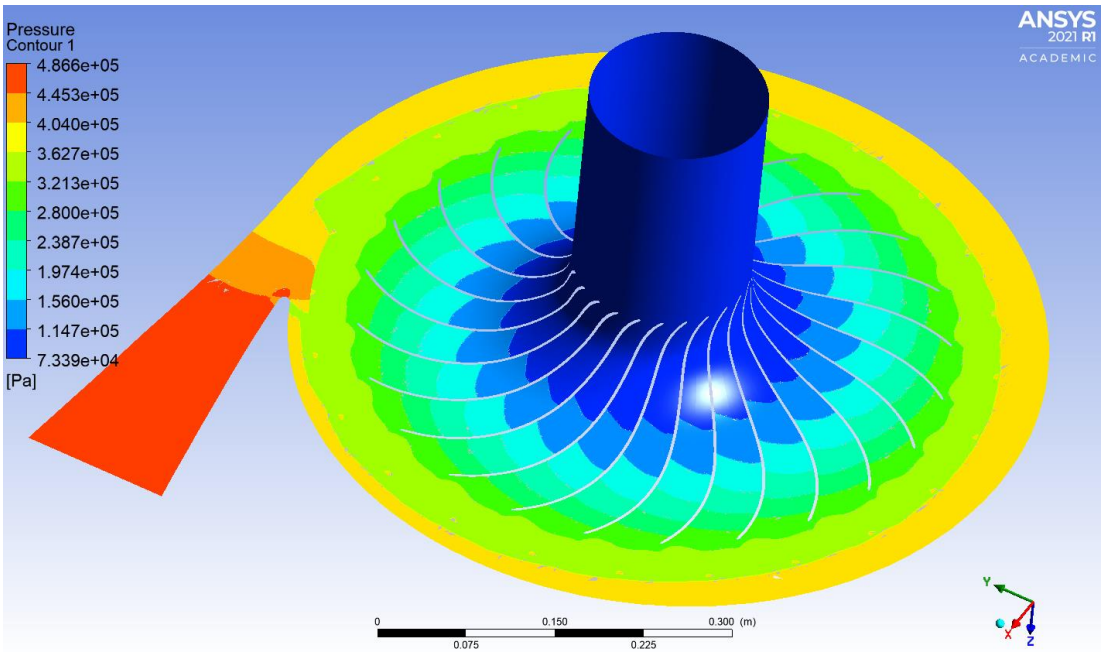

Figure 16: Local pressure distribution in the midspan of the compressor.

As seen from figure, while there is 1 bar pressure at the inlet, there is an approximate static pressure of 4.86 bar at the outlet. Considering the compressor requirements, this pressure value is within an acceptable range.

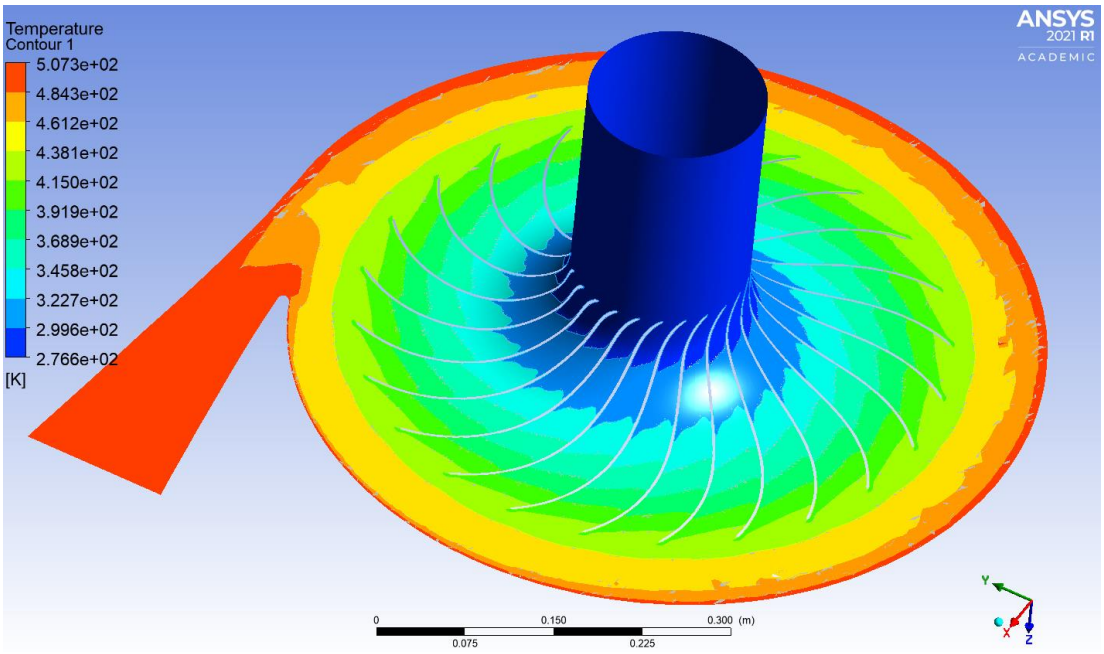

Figure 17: Local temperature distribution in the midspan of the compressor.

As seen from figure, while the inlet temperature is 20°C, the outlet temperature is approximately 234°C. This value is quite close to the outlet temperature obtained from the actual thermodynamic analysis.

CONCLUSIONS

This report has been prepared in the scope of the Senior Design Project of Yasin Yıldız, a final-year student in the Department of Mechanical Engineering at Istanbul Technical University. Due to the satisfactory performance of the designed turbocharger's compressor section, the report focuses solely on the compressor design.

As part of the compressor design process, thermodynamic analysis was initially conducted to determine the inlet and outlet state variables of the compressor. Subsequently, the compressor was aerodynamically designed and its geometry was established. Finally, CFD simulations were performed to assess its performance. The compressor requirements and the performance values obtained from CFD simulations closely match each other. In conclusion, the thermodynamic and aerodynamic design of a 500 kW compressor capable of delivering 5 bar pressure, meeting the requirements, has been successfully accomplished.

REFERENCES

Aungier, R. H. (2000). *Centrifugal compressors: A strategy for aerodynamic design and analysis*. American Society of Mechanical Engineers.

Balje´, O. E. (1962). A study on design criteria and matching of turbomachines: Part A—similarity relations and design criteria of turbines. *Journal of Engineering for Power*, *84*(1), 83–102. https://doi.org/10.1115/1.3673386

Bathie, W. W. (1996). *Fundamentals of Gas Turbines*. J. Wiley.

Chen, T., Zhuge, W., Zheng, X., Zhang, Y., & He, Y. (2009). Turbocharger design for a 1.8 liter turbocharged gasoline engine using an integrated method. *Volume 7: Turbomachinery, Parts A and B*. https://doi.org/10.1115/gt2009-59951

Cumpsty, N. A. (2004). *Compressor aerodynamics*. Krieger Publishing Company.

Gunees, M. (2022). *Performance Enhancement of Turbocharger Centrifugal Compressor* (thesis).

Ingram, G. (2009). *Basic Concepts in Turbomachinery*. Grant Ingram & Ventus Publishing.

Korpela, S. A. (2020). *Principles of turbomachinery*. Wiley.

Nguyen-Schäfer, H. (2015). *Rotordynamics of automotive turbochargers*. Springer International Publishing.

Peng, W. W. (2008). *Fundamentals of turbomachinery*. Wiley.

Topcu, M. T. (2018). *Dizel bir araçta tahliyekapaklı turboşarjın tasarım ve analizi* (thesis).

Tosto, F. (2018). *Investigation of performance and surge behavior of centrifugal compressors through CFD simulations* (thesis).

Whitfield, A., & Baines, N. C. (2002). *Design of radial turbomachines*. Longman.

Yılmaz, H. İ. (2019). *Dizel araçlarda çift kademeli turboşarjır tasarımı ve analizi* (thesis).

Zhang, Y., Chen, T., Zhuge, W., Zhang, S., & Xu, J. (2010). An integrated turbocharger design approach to improve engine performance. *Science in China Series E: Technological Sciences*, *53*(1), 69–74. https://doi.org/10.1007/s11431-009-0421-9

Çanga, Z. (2016). *Theoretical and experimental analysis of turbocharger in tractor engines* (thesis).

Çıbıkçı, K. Ç. (2017). *Motorlarda turboşarj sisteminin analizi* (thesis).

ÖZ, G. C. (2013). *Ağır ticari motor için turboşarj seçimi ve egzoz manifoldu tasarımı ve imalatı* (thesis).